An Ergo-Interactive Framework for Human-Robot Collaboration Via Learning From Demonstration

Zhiwei Liao, *Student Member, IEEE*, Marta Lorenzini, *Member, IEEE*, Mattia Leonori, Fei Zhao, *Member, IEEE*, Gedong Jiang, and Arash Ajoudani, *Member, IEEE*

***Abstract*—This work presents an ergonomic and interactive human-robot collaboration (HRC) framework, through which new collaborative skills are extracted from a one-shot human demonstration and learned through Riemannian dynamic movement primitives (DMP). The proposed framework responds to human-robot interaction forces to adapt to the task requirements, while generating virtual "ergonomic forces" that guide the human toward more ergonomic postures, based on online monitoring of a kinematics-based index. The resulting motion is then integrated into the learned task trajectories. The framework is implemented on a mobile manipulator with a weighted whole-body Cartesian velocity controller, which meets the needs of large-scale HRC. To evaluate the proposed framework, a multi-subject experiment involving a human-robot co-carrying task is conducted. The performance of the ergo-interactive control in terms of task performance and ergonomics adaptation is verified under different experimental conditions. This is followed by a comparative statistical analysis. The experimental results show that the learned trajectory can be reproduced and generalized to several targets and adjusted online according to human preferences and ergonomics.**

***Index Terms*—Human-robot collaboration, Riemannian-based DMP, human ergonomics, robot dynamic adaptation.**

I. Introduction

HUMAN-ROBOT collaboration (HRC), which blends the complementarity between humans and robots, has recently earned an increasing slope in the research community's interest [1]. Humans have better dexterity, flexibility, and decision-making capabilities. Meanwhile, robots, with their superior precision, repeatability, and power, can be widely applied in high-accuracy and high-effort tasks. The synergy between them exhibits an enormous potential in safeguarding human health as well as improving task efficiency, both in domestic and industrial scenarios.

One of the major challenges is the collaboration policy design and corresponding programming of HRC, the complexity of which increases with the requirements of the task, especially in unstructured environments. The lack of fast-programming adaptive approaches for robots actively collaborating with humans restricts them from entering highly dynamic small and medium-sized factories and people's daily life. To reduce the threshold for the use of collaborative robots (CoBots), learning from human demonstration (LfHD) takes a feasible way and has received extensive attention in recent years [2]. Multi-agent tasks can be learned from human-human demonstrations and then transferred to human-robot teams, providing fast-programming HRC policies. Several LfHD-based HRC applications have been proposed so far, including object co-carrying [3], [4], [5], [6], handover [7], [8], co-assembly [9], [10], and co-processing [11]. Focusing on contact-rich HRC tasks, online modules have been also developed to dynamically adjust the learned behavior and adapt it to new conditions. For instance, [4] focuses on learning adaptive policies from demonstrations by combining machine learning and haptic information in human-robot co-carrying. In [6], an online adaptive module is integrated into the Gaussian mixture model to make the robot switch its leader and follower roles, according to the interaction forces and velocities, while mastering the learned skills. Similarly, in [11], the robot can adapt its collaborative roles to human preferences through interaction in a co-sawing task, but a human-in-the-loop approach is employed to directly teach robots to collaborate with humans.

The aforementioned studies are mainly focused on robot role and trajectory adaptation based on human interaction. On the other hand, the learned skills are individualized, i.e. based on the human demonstrator. As a result, they may not fit other partners with different heights, body lengths, behaviors, etc., and negatively affect human physical ergonomics. Indeed, a different human partner may adopt awkward postures to follow the learned trajectory. A human interaction-based approach may not be sufficient to address the ergonomic needs of the users, who may not be fully aware of them. Nevertheless, non-ergonomic configurations are one of the major risk factors for the development of musculoskeletal disorders (MSD), which, according to the European Agency for Safety and Health at Work

Manuscript received 20 June 2023; accepted 12 October 2023. Date of publication 30 October 2023; date of current version 28 November 2023. This letter was recommended for publication by Associate Editor T. Tsuji and Editor J.-H. Ryu upon evaluation of the reviewers' comments. This work was supported in part by the National Natural Science Foundation of China under Grant 52175029, and in part by European Research Council starting grant Ergo-Lean under Grant 850932. The work of Zhiwei Liao was supported by China Scholarship Council. *(Corresponding author: Fei Zhao.)*

This work involved human subjects or animals in its research. Approval of all ethical and experimental procedures and protocols was granted by ethics committee Azienda Sanitaria Locale Genovese N.3 under Application No. IIT_HRII_ERGOLEAN 156/2020, and performed in line with the Helsinki Declaration.

Zhiwei Liao is with the State Key Laboratory for Manufacturing Systems Engineering, Shaanxi Key Laboratory of Intelligent Robots, and School of Mechanical Engineering, Xi'an Jiaotong University, Xi'an 710049, China, and also with HRI2 Laboratory, IIT, 16163 Genova, Italy (e-mail: liao.zhiwei@stu.xjtu.edu.cn).

Marta Lorenzini, Mattia Leonori, and Arash Ajoudani are with HRI2 Laboratory, IIT, 16163 Genova, Italy (e-mail: marta.lorenzini@iit.it; mattia.leonori@iit.it; arash.ajoudani@iit.it).

Fei Zhao and Gedong Jiang are with the State Key Laboratory for Manufacturing Systems Engineering, Shaanxi Key Laboratory of Intelligent Robots, and School of Mechanical Engineering, Xi'an Jiaotong University, Xi'an 710049, China (e-mail: ztzhao@mail.xjtu.edu.cn; gdjiang@mail.xjtu.edu.cn).

This letter has supplementary downloadable material available at https://doi.org/10.1109/LRA.2023.3328366, provided by the authors.

Digital Object Identifier 10.1109/LRA.2023.3328366

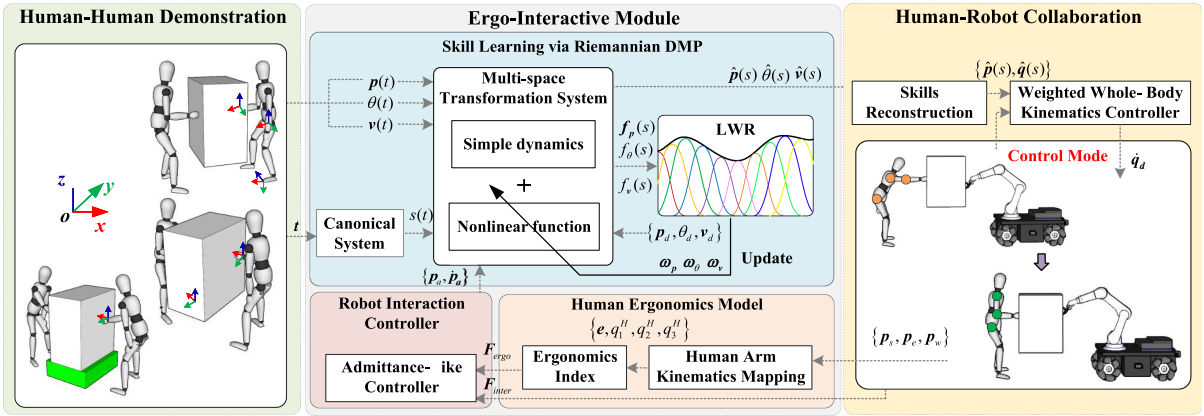

Fig. 1. Diagram of the proposed ergonomic and interactive (ergo-interactive) HRC framework via LfHD.

(EU-OSHA), affect approximately three out of five workers and pose enormous economic and social costs [12].

To address this issue, CoBots have broadened their application to improve human ergonomics, especially for postural correction [13]. For instance, a whole-body dynamic model was proposed in [14] to estimate human overloading joint torques during co-manipulation tasks and minimize them through robot guidance to achieve more ergonomic postures. Similarly, [15] presents a virtual element method to assess human ergonomics and make the robot optimize human configurations. For the HRC co-carrying task, the authors in [16] developed a novel metric that combines muscle activation and ergonomics of the human arm to online predict human comfort and analyze manipulability. Instead, the work in [17] estimates human ergonomics based on the Rapid Entire Body Assessment (REBA) method [18], and the robot adjusts human configurations along an optimized action sequence planned by an informed graph search algorithm. Several studies have been proposed in the literature to model and estimate the human physical load and mitigate it through HRC. However, the robot thereof only fulfills the role of a caregiver that ergonomically adjusts human posture, rather than a partner with its own active job that performs specific tasks in a shared workstation.

To the best of our knowledge, there are still no works that integrate human ergonomics as a dynamic factor into LfHD to modify the learned skills and thus focus on both human state monitoring and the human-robot shared task. Hence, the purpose of this letter is to propose an ergonomic and interactive LfHD-based HRC framework that (i) teaches robots to collaborate with humans and gain new skills from human demonstration, and (ii) integrates not only human preferences[1] but also human ergonomics in the robot control to online modify the learned skills. In our framework, the skill-learning method provides a fast-programming way for robots to master collaboration skills, and the online ergo-interactive module integrates the merits of humans and robots so that they can supervise each other during collaboration, accomplishing tasks while ensuring human ergonomics to reduce the risk of MSD.

The remainder of this letter is structured as follows: Section II proposes the whole framework including skill learning, the estimation of human preferences and ergonomics, and robot adaptive control. Section III conducts a human-robot co-carrying experiment and discusses the experimental results. Section IV concludes this letter.

[1]In this letter, we refer to human preferences as the human willingness to modify the robot trajectory through interaction forces exchange with it.

II. Ergonomic and Interactive Human-Robot Collaboration Learning Framework

The proposed framework (see Fig. 1) is composed of three blocks: human-human demonstration, ergo-interactive module, and human-robot collaboration. The ergo-interactive module, in turn, is composed of three modules: skill learning via DMP, human ergonomics, and robot interaction controller. In the human-human demonstration block, a task-related trajectory, including the position and orientation of the human arm, is recorded. In the skill learning module, the Riemannian-based DMP is used to encode the recorded position and orientation in Cartesian space and Riemannian manifold, respectively, and define reference trajectories. The HRC block implements a whole-body controller to execute such reference trajectories and carry out the task. In the human ergonomics module, a human upper-body model and kinematics-based indexes are used to online evaluate the body configuration of the human during the HRC task and compute virtual forces for posture correction. To online adapt the robot behavior to human ergonomics and preferences during HRC, the robot interaction controller module features an admittance-like controller. This module takes as input the dynamic interaction forces directly resulting from the HRC block and the virtual forces from the human ergonomics module and adjusts the reference trajectories accordingly. These components are explained in detail in the following subsections.

A. Skill Learning

In our previous work [19], a Riemannian-based DMP was developed to simultaneously transfer human skills of position and orientation in multiple spaces, in which the orientation is represented by quaternion and further decoupled as an angle and a specific axis. Hereinafter we represent these parameters as angle-quaternion and axis-quaternion, respectively.

For those skills related to the Cartesian space (position $\boldsymbol{p} \in \mathbb{R}^3$ and angle-quaternion $\theta \in \mathbb{R}$), the mathematical model of the

transformation system is formulated as follows:

$$\tau \begin{bmatrix} \dot{\boldsymbol{z}}_p \\ \dot{z}_\theta \end{bmatrix} = \alpha_c \left(\beta_c \left(\begin{bmatrix} \boldsymbol{p}_g \\ \theta_g \end{bmatrix} - \begin{bmatrix} \boldsymbol{p} \\ \theta \end{bmatrix} \right) - \begin{bmatrix} \boldsymbol{z}_p \\ z_\theta \end{bmatrix} \right) + \begin{bmatrix} \boldsymbol{f}_{\boldsymbol{p}}(s) \\ f_\theta(s) \end{bmatrix},$$
$$\tau \begin{bmatrix} \dot{\boldsymbol{p}} \\ \dot{\theta} \end{bmatrix} = \begin{bmatrix} \boldsymbol{z}_p \\ \boldsymbol{z}_\theta \end{bmatrix}, \tag{1}$$

where $\boldsymbol{p} = [p_x, p_y, p_z]^T$, $\boldsymbol{z}_p = [z_{p_x}, z_{p_y}, z_{p_z}]^T$ and $\dot{\boldsymbol{z}}_p = [\dot{z}_{p_x}, \dot{z}_{p_y}, \dot{z}_{p_z}]^T$ are the position, velocity, and acceleration, along the x-, y-, and z- axes, respectively. θ, z_θ, and $\dot{z}_\theta$ are the angle-quaternion and its corresponding angular velocity and acceleration, respectively. $\boldsymbol{f}_{\boldsymbol{p}}(s)$ and $f_\theta(s)$ are the nonlinear functions, where s is the phase variable. τ is a time scaling factor, which is used to adjust task duration. α_c and β_c are positive constants guaranteeing that $\boldsymbol{p}$ and θ will finally converge to their targets $\boldsymbol{p}_g$ and θ_g.

For the axis-quaternion ($\boldsymbol{v} \in \mathcal{S}^2$) which is located on the 2-D sphere manifold, the extended transformation system is developed as follows:

$$\tau \dot{\lambda}_i = \alpha_r \left(\beta_r \mathrm{d}\left(\boldsymbol{v}_g, \boldsymbol{v}_i\right) - \lambda_i \right) + \mathrm{d}\left(\boldsymbol{v}_g, \boldsymbol{v}_0\right) f_{\boldsymbol{v}}\left(s_i\right),$$
$$\tau \dot{\boldsymbol{v}}_i = \tau \frac{\mathrm{d}\left(\boldsymbol{v}_{i+1}, \boldsymbol{v}_i\right)}{\mathrm{d}t} = \lambda_i, \tag{2}$$

where $\mathrm{d}(\boldsymbol{v}_1, \boldsymbol{v}_2) \in \mathbb{R}$ represents the geodesics between $\boldsymbol{v}_1 \in \mathcal{S}^2$ and $\boldsymbol{v}_2 \in \mathcal{S}^2$, equal to $\arccos(\boldsymbol{v}_1^{\mathrm{T}} \boldsymbol{v}_2)$. $\boldsymbol{v}_i = \boldsymbol{v}(s_i)$ is the vector $\boldsymbol{v}$ in the ith phase s_i. $\lambda_i \in \mathbb{R}$ is the scaled velocity term. $\boldsymbol{v}_0$ and $\boldsymbol{v}_g$ are the initial and target vectors, respectively. $f_{\boldsymbol{v}}(s_i) \in \mathbb{R}$ is a nonlinear function. α_r and β_r are positive constants ensuring the convergence of $\boldsymbol{v}_i$ to the targets $\boldsymbol{v}_g$.

In (1) and (2), the shape of each skill is determined by the nonlinear terms $f_p(s)$ and $f_{\boldsymbol{v}}(s)$ which are fitted with LWR by using a linear combination of N RBFs as:

$$f\left(s\right) = \frac{\sum_{i=1}^{N} \omega_i \Psi_i\left(s\right)}{\sum_{i=1}^{N} \Psi_i\left(s\right)} s, \tag{3}$$

$$\Psi_i\left(s\right) = \exp\left(-h_i \left(s - c_i\right)^2\right), \tag{4}$$

where c_i, h_i and ω_i represent the center, width, and weight of the ith RBF, respectively.

To guarantee the temporal consistency among different skills and avoid the explicit time dependency of the system, the phase variable s is determined by the first-order linear dynamic system, that is, the canonical system:

$$\tau \dot{s} = -\alpha_s s, \tag{5}$$

where $s \in [0, 1]$, $s(0) = 1$, $\dot{s}$ denotes the derivative of s, and α_s is a positive constant.

On this basis, as shown in Fig. 1, the skills are encoded by the weight matrices $\{\boldsymbol{\omega}_x, \boldsymbol{\omega}_y, \boldsymbol{\omega}_z, \boldsymbol{\omega}_\theta, \boldsymbol{\omega}_{\boldsymbol{v}}\}$ and the learned DMP can online calculate the next-step pose according to the targets $\{p_{x,d}, p_{y,d}, p_{z,d}, \theta_d, \boldsymbol{v}_d\}$, the current phase variable s, and the weight matrices. For the details, please refer to [19].

B. Human Ergonomics

In this letter, the human is involved in a co-carrying task, as shown in Fig. 2(a). The pelvis of the human body is set as the base frame and three degrees of freedom (DoFs) are considered:

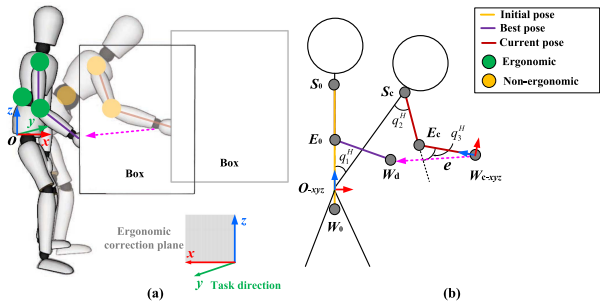

Fig. 2. (a) Human co-carrying task and (b) upper body kinematic model. The ergonomic correction-related plane (xoz) and the task-related axis (y), which is normal to xoz, are highlighted.

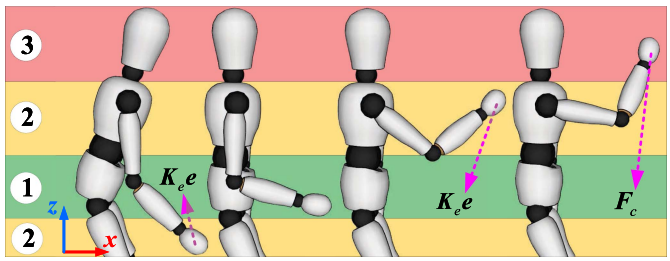

Fig. 3. The areas of the human workspace. 1: Ergonomic and supervised, 2: Not-ergonomic but supervised, 3: Not-ergonomic and not-supervised.

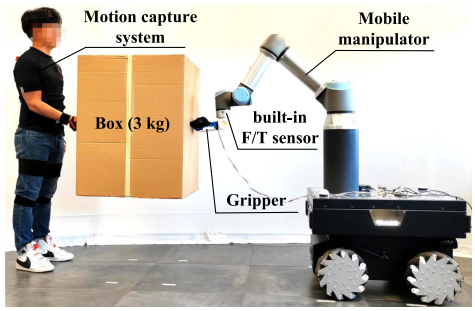

Fig. 4. Experimental setup for Human-robot co-carrying.

the back, shoulder, and elbow flexion-extension. To perform the task, the human may adopt different body configurations, which can be considered more or less detrimental for these joints, as highlighted in green and yellow spheres in the picture. To both take into account human physical ergonomics and minimize the impact on task completion, we assume that the main direction of the task, along which the human partner can follow the robot, is the y-axis of the human body base frame (normal to the sagittal xoz plane), and we consider ergonomic guidance in the xoz plane. In particular, our objective is to prevent incorrect postures of the human upper body in the sagittal plane. The human kinematic model and ergonomic index that we implement for this purpose are described as follows.

1) Human Upper Body Kinematic Model: Fig. 2(b) depicts the human upper body kinematic mapping to the xoz plane to obtain a sagittal model. Given the positions of the shoulder, elbow, and wrist joints, and based on screw theory, the angles of the mentioned movements can be calculated.

As shown in Fig. 2(b), the initial configuration of the human upper body is set as $OS_0E_0W_0$, in which $q_1^H = 0$, $q_2^H = 0$, and

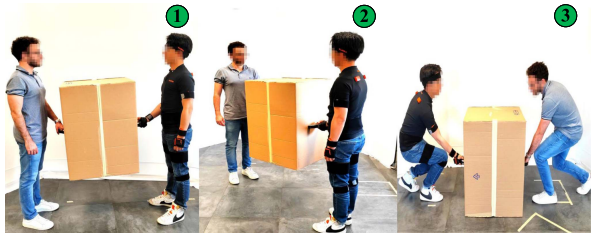

Fig. 5. Human-human co-carrying demonstration (1: Initial state, 2: Intermediate state, 3: Final state).

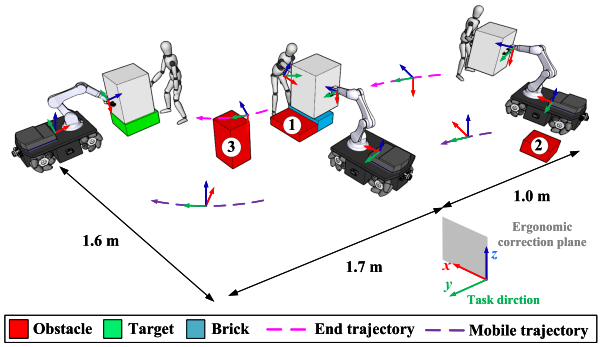

Fig. 6. Human-robot co-carrying task setting.

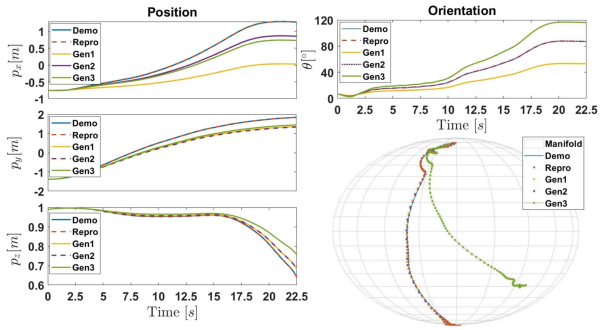

Fig. 7. Skill learning, reproduction, and generalization (Demo: Demonstrated curve, Repro: Reproduced curve, gen(i): Generalized curve for the target(i).).

$q_3^H = 0$. Let us assume the current configuration of the human upper body as $OS_cE_cW_c$ and the positions of the shoulder, elbow, and wrist joints as $\boldsymbol{p}_s$, $\boldsymbol{p}_e$, and $\boldsymbol{p}_w$, respectively. Thus, q_1^H, q_2^H, and q_3^H can be calculated as follows:

$$q_1^H = \text{sgn}(\boldsymbol{p}_{s,x}) \arccos\left(\left(\frac{\boldsymbol{p}_s}{\|\boldsymbol{p}_s\|}\right)^T \boldsymbol{v}_z\right), \tag{6a}$$

$$q_2^H = \text{sgn}(\boldsymbol{p}_{e,x} - \boldsymbol{p}_{s,x}) \arccos\left(\left(\frac{\boldsymbol{p}_e - \boldsymbol{p}_s}{\|\boldsymbol{p}_e - \boldsymbol{p}_s\|}\right)^T \left(-\frac{\boldsymbol{p}_s}{\|\boldsymbol{p}_s\|}\right)\right), \tag{6b}$$

$$q_3^H = \arccos\left(\left(\frac{\boldsymbol{p}_e - \boldsymbol{p}_s}{\|\boldsymbol{p}_e - \boldsymbol{p}_s\|}\right)^T \left(\frac{\boldsymbol{p}_w - \boldsymbol{p}_e}{\|\boldsymbol{p}_w - \boldsymbol{p}_e\|}\right)\right), \tag{6c}$$

where $\boldsymbol{p}_{s,x}$, $\boldsymbol{p}_{e,x}$, and $\boldsymbol{p}_{w,x}$ represent the positions of the shoulder, elbow, and wrist joints on the x- axis, respectively. $\boldsymbol{v}_z = [0,0,1]^T$ denotes the vector of the z- axis and sgn stands for the sign function. According to the kinematic model in Fig. 2(b), the rotational axes are $\boldsymbol{\omega}_1 = [0,1,0]^T$, $\boldsymbol{\omega}_2 = [0,-1,0]^T$, and $\boldsymbol{\omega}_3 = [0,-1,0]^T$. The arbitrary points on each axis are set as $\boldsymbol{p}_1 = [0,0,0]^T$, $\boldsymbol{p}_2 = [0,0,\boldsymbol{p}_{s,y}]^T$, and $\boldsymbol{p}_3 = [0,0,\boldsymbol{p}_{s,z} - l_{se}]^T$, respectively, in which $\boldsymbol{p}_{s,z}$ is the position of the shoulder joint on the z- axis, and l_{se} is the length from the shoulder joint to the elbow joint. Thus, the screws of each joint can be calculated as $\boldsymbol{\xi}_i = [-\hat{\boldsymbol{\omega}}_i \boldsymbol{p}_i,\ \boldsymbol{\omega}_i]^T$.

The kinematics of the human upper body can be derived as:

$$\boldsymbol{R}^{\hat{\omega} q^H} = \boldsymbol{I} + \hat{\boldsymbol{\omega}} \sin\left(q^H\right) + \hat{\boldsymbol{\omega}}^2 \left(1 - \cos\left(q^H\right)\right), \tag{7}$$

$$\boldsymbol{T}^{\hat{\omega} q^H} = \left(\boldsymbol{I} - \boldsymbol{R}^{\hat{\omega} q^H}\right)\left(\hat{\boldsymbol{\omega}}\left(-\hat{\boldsymbol{\omega}}\boldsymbol{p}\right)\right), \tag{8}$$

$$e^{\hat{\xi} q^H} = \begin{bmatrix} \boldsymbol{R}^{\hat{\omega} q^H} & \boldsymbol{T}^{\hat{\omega} q^H} \\ \boldsymbol{0}^{1\times 3} & 1 \end{bmatrix}, \tag{9}$$

$$\boldsymbol{g}_{st} = e^{\hat{\boldsymbol{\xi}}_1 q_1^H} e^{\hat{\boldsymbol{\xi}}_2 q_2^H} e^{\hat{\boldsymbol{\xi}}_3 q_3^H} \boldsymbol{g}_0, \tag{10}$$

where $\hat{\boldsymbol{\omega}} \in so(3)$ is a 3×3 skew-symmetric matrix, $\boldsymbol{g}_0$ and $\boldsymbol{g}_{st}$ are the initial and current poses of the wrist joint, wherein $\boldsymbol{g}_0 = \begin{bmatrix} \boldsymbol{I}^{3\times 3} & \boldsymbol{T}_0^{3\times 1} \\ \boldsymbol{0}^{1\times 3} & 1 \end{bmatrix}$, $\boldsymbol{T}_0 = [0,0,\boldsymbol{p}_{s,z} - l_{se} - l_{ew}]^T$, and l_{ew} is the length from the elbow to the wrist joints.

2) Ergonomic Index: Based on the mentioned kinematic model, we define an ergonomic index as the displacement from the most ergonomic human upper body configuration and proximity to mechanical joint limits [20].

$$\gamma(q^H) = \frac{\left\|q^H - q_d^H\right\|}{q_{\max}^H - q_d^H}, \tag{11}$$

where $\gamma(q^H) \in [0,1]$ denotes the ergonomic index w.r.t. the current angle q^H. q_d^H and $q_{\max}^H$ are the desired angle and the joint limit, respectively. We select their maximum value $\gamma_{\max}$ as the overall ergonomic index

$$\gamma_{\max} = \max(\gamma(q_1^H), \gamma(q_2^H), \gamma(q_3^H)), \tag{12}$$

to minimize the risk associated with each joint. As shown Fig. 2(b), the distance $\boldsymbol{e}$ from the current to the best positions of the wrist joint can be calculated as follows:

$$\boldsymbol{e} = \boldsymbol{T}^{\hat{\omega} q_d^H} - \boldsymbol{T}^{\hat{\omega} q^H}. \tag{13}$$

C. Robot Controller

This letter employs a 9-Dofs mobile manipulator for large-space HRC with a weighted whole-body kinematics controller. Since the considered platform is a redundant system, its desired joint velocities $\dot{\boldsymbol{q}}_d \in \mathbb{R}^{6+3}$ can be obtained by solving a Hierarchical Quadratic Program (HQP) problem consisting of two tasks. HQP approaches in robotics are well-known for their stability due to the convex optimization and the inclusion of constraints that ensure the system operates within certain bounds or adheres to specific constraints. The primary task is to guarantee the tracking accuracy of the desired end-effector trajectory $(\boldsymbol{p}_d, \dot{\boldsymbol{p}}_d)$, while the secondary task is realized in the null space of the primary one [21], as:

$$\dot{\boldsymbol{q}}_d = \dot{\boldsymbol{q}}_{d,1} + \boldsymbol{J}_N(\boldsymbol{q})\dot{\boldsymbol{q}}_{d,2}, \tag{14}$$

where $\dot{\boldsymbol{q}}_d \in \mathbb{R}^9$, $\dot{\boldsymbol{q}}_{d,1} \in \mathbb{R}^9$, and $\dot{\boldsymbol{q}}_{d,2} \in \mathbb{R}^9$ denote the desired, primary, and secondary joint velocities. $\boldsymbol{J}_N(\boldsymbol{q}_{d,1}) \in \mathbb{R}^{9\times 9}$ is the null-space Jacobian.

On this basis, the primary task is realized by formulating the following cost function [22]:

$$\boldsymbol{L}_1 = \frac{1}{2}\left\|\dot{\boldsymbol{x}}_d + \boldsymbol{K}(\boldsymbol{x}_d - \boldsymbol{x}) - \boldsymbol{J}(\boldsymbol{q})\dot{\boldsymbol{q}}\right\|^2_{\boldsymbol{W}_1} + \frac{1}{2}\left\|k\dot{\boldsymbol{q}}\right\|^2_{\boldsymbol{W}_2}, \tag{15}$$

where $\dot{\boldsymbol{q}} \in \mathbb{R}^9$ denotes the optimized joint velocity. $\boldsymbol{x} \in \mathbb{R}^6$, and $\boldsymbol{x}_d \in \mathbb{R}^6$ represent the current and desired end-effector poses. $\boldsymbol{J}(\boldsymbol{q}) \in \mathbb{R}^{6\times 9}$ is the whole-body Jacobian. $\boldsymbol{W}_1 \in \mathbb{R}^{6\times 6}$, $\boldsymbol{W}_2 \in \mathbb{R}^{9\times 9}$, and $\boldsymbol{K} \in \mathbb{R}^{6\times 6}$ are diagonal positive definite matrices, and $k > 0$ is a damping factor. These default settings determine the tracking accuracy of end-effector poses and the numerical stability of solutions.

The cost function for the secondary task is formulated to keep the manipulator close to the default joint configuration and the mobile base close to the desired trajectory as:

$$\boldsymbol{L}_2 = \frac{1}{2}\left\|\boldsymbol{q}_{def} - \boldsymbol{q}\right\|^2_{\boldsymbol{W}_3}, \tag{16}$$

where $\boldsymbol{W}_3 \in \mathbb{R}^{9\times 9}$ is a diagonal positive semi-definite matrix to determine the priority of the mobile base and the manipulator. $\boldsymbol{q}_{def} \in \mathbb{R}^9$ denotes the default settings of the mobile base and manipulator. We set $\boldsymbol{q}_{def} = \left[\boldsymbol{q}_{pel} \in \mathbb{R}^3, \boldsymbol{q}_0 \in \mathbb{R}^6\right]$, in which $\boldsymbol{q}_{pel}$, including the position along x- and y- axes and the rotated angle along z- axis, is calculated through the demonstrated motion of the subject's pelvis joint, and $\boldsymbol{q}_0$ is the default joint configuration of the manipulator. The joint velocities of the secondary task are computed as the negative gradient w.r.t. $\boldsymbol{q}$.

It is worth emphasizing here that the collaborative motion planning of the manipulator and the mobile base is critical but tedious work. Existing researches achieve feasible manipulator-mobile configurations in large-space operations mostly by manually adjusting parameters in (15) and (16) of the controller. This letter proposes a new way to intuitively plan the manipulator-mobile configurations via skill transfer from human demonstration. The wrist joint trajectory can be used as the desired pose of the robot end-effector, and the pelvis joint motion can be used as a reference for the mobile base.

D. Robot Ergo-Interactive Behaviour

To online adjust the HRC learned trajectory by considering human ergonomics and preferences, we develop an admittance-like controller. In our scenario, human preferences can be represented by the human-robot interaction force $\boldsymbol{F}_{inter}$ directly measured through an F/T sensor on the robot end-effector, while the ergonomic correction can be translated in a force $\boldsymbol{F}_{ergo}$ calculated as follows:

$$\boldsymbol{F}_{ergo} = \begin{cases} 0, & \gamma_{\max} \le \gamma_{\text{thr}} \\ \boldsymbol{K}_e\boldsymbol{e}, & \gamma_{\max} > \gamma_{\text{thr}},\ \|\boldsymbol{e}\| \le \|\boldsymbol{e}\|_{\text{thr}} \\ \text{sgn}(\boldsymbol{e})\boldsymbol{F}_c, & \|\boldsymbol{e}\| > \|\boldsymbol{e}\|_{\text{thr}} \end{cases}, \tag{17}$$

where $\gamma_{\max}$ denotes the ergonomic index (11), $\|\boldsymbol{e}\|$ denotes the norm of $\boldsymbol{e}$ (12). γ_{thr} and $\|\boldsymbol{e}\|_{\text{thr}}$ are the thresholds w.r.t. $\gamma_{\max}$ and $\|\boldsymbol{e}\|$, respectively. $\boldsymbol{K}_e \in \mathbb{R}^{3\times 3}$ is a diagonal positive matrix, $\boldsymbol{F}_c \in \mathbb{R}^3$ is set empirically to a constant positive vector and the sign of $\boldsymbol{F}_{ergo}$ depends on the error direction $\boldsymbol{e}$.

On this basis, as shown in Fig. 3, three areas are defined in the human workspace, i.e., ergonomic and supervised (green), not-ergonomic but supervised (yellow), and not-ergonomic and not-supervised (red). The ergonomic and supervised areas are determined by $\gamma_{\max}$ and $\|\boldsymbol{e}\|$, respectively. The watershed values are task-oriented. When $\gamma_{\max}$ is under the threshold (ergonomic and supervised area) only the guidance to follow the learned trajectory is provided. Instead, when $\gamma_{\max}$ exceeds the threshold (not-ergonomic area), the robot applies also a force that drives the human body to the most ergonomic configuration. The higher is $\|\boldsymbol{e}\|$, major is the correction. When $\|\boldsymbol{e}\|$ exceeds the predefined threshold, meaning that the human is significantly deviating from the robot trajectory (not-supervised area), $\boldsymbol{F}_{ergo} = \boldsymbol{F}_c$. This keeps the ergonomic correction fixed and allows us to avoid a huge feedback force. Unlike the supervised area, where the subjects are mostly following the Cobot, in the not-supervised area, they may want to impose their preferences and modify the path. It should be noted that human preferences are considered through $\boldsymbol{F}_{inter}$ in all three areas.

Thus, the combined forces and the augmented positions and velocities can be calculated as:

$$\boldsymbol{F} = \boldsymbol{F}_{ergo} + \boldsymbol{F}_{inter}, \tag{18}$$

$$\dot{\boldsymbol{p}}_a(t) = \boldsymbol{D}_d^{-1}\left(\boldsymbol{F} - \boldsymbol{K}_d\boldsymbol{p}_a(t-1)\right), \tag{19}$$

$$\boldsymbol{p}_a(t) = \boldsymbol{p}_a(t-1) + \dot{\boldsymbol{p}}_a(t)\Delta t, \tag{20}$$

where $\boldsymbol{p}_a$ and $\dot{\boldsymbol{p}}_a$ represent the augmented position and velocity through the admittance controller, respectively. $\boldsymbol{K}_d$ and $\boldsymbol{D}_d$ represent the stiffness and damping of the controller. Δt denotes the interval time which is dependent on the robot control frequency f, i.e., $\Delta t = 1/f$.

Therefore, the learned trajectory can be adjusted online as:

$$\hat{\boldsymbol{p}} = \boldsymbol{p} + \boldsymbol{p}_a\Delta t, \tag{21}$$

$$\hat{\boldsymbol{z}} = \boldsymbol{z} + \dot{\boldsymbol{p}}_a\frac{\Delta t}{\tau}, \tag{22}$$

where $\boldsymbol{p}$ and $\boldsymbol{z}$ denote the learned position and velocity in (1) while $\hat{\boldsymbol{p}}$ and $\hat{\boldsymbol{z}}$ are the adjusted position and velocity. Since the update frequency of (1) matches the robot control frequency, Δt is introduced in (21) and (22) to discretize the augmented motion at the position and velocity level and obtain the displacement for each control loop.

III. Experiments

To validate the proposed framework, an experimental campaign was conducted with a human-robot co-carrying task.

A. Experimental Setup

The experimental setup is illustrated in Fig. 4. A wearable motion-capture (MoCap) system (Xsens MVN suit, 60 Hz), including seventeen inertial measurement unit (IMU) sensors, was used to measure the motion of the human body. A Kairos+ 16E was used as the mobile manipulator. It includes a 3-DoFs Omni-directional Robotnik SUMMIT-XL STEEL mobile base, a 6-DoFs Universal Robot UR16e arm, and a 1-DoF Pisa/IIT Softhand. The Robot arm had a built-in F/T sensor that measures the interactive wrenches between the robot and the environment. A whole-body velocity controller running at 500 Hz was employed.

B. Experimental Protocols

Three experiments were conducted. First, a one-shot human-human demonstration was executed to extract HRC skills. Then, the skills were learned and generalized to different targets. Finally, a multi-subject experiment was performed to validate the robot's ergo-interactive behaviour. [2]

1) Human-Human Demonstration: One of the authors (height: 1.67 m, arm length: 0.49 m) first demonstrated the co-carrying task (Fig. 5) with another human partner. The trajectories of the wrist and pelvis joints w.r.t. the world frame of the MoCap system were recorded.

2) Skill Learning and Generalization: The Riemannian-based DMP was introduced to encode the trajectory including the multi-space skills of position (in Cartesian space) and orientation (on the Riemannian manifold). According to (1) and (2), the robot execution time can be determined by the temporal scaling factor τ. Hence, the demonstrated trajectories were fitted through several RBFs, and the reproduced and generalized trajectories (noted by Gen in this letter) were calculated online according to the robot current poses, new targets, and phase variables.

Prior to the multi-subject experiments, the learning capability of the Riemannian-based DMP was evaluated. One of the demonstrators collaborated with the robot to put the box on three new targets with various positions and orientations.

3) Robot Ergo-Interactive Behaviour Evaluation: After that, we selected one of the targets (see Gen2 in Fig. 7) to test the robot adaptation based on the presented framework. Six subjects (heights: $\{1.70 \pm 0.18\,\mathrm{m}\}$, arm lengths: $\{0.54 \pm 0.09\,\mathrm{m}\}$) were recruited [3] and asked to perform the HRC task three times. The task setting is shown in Fig. 6.

In the first trial (NA), they collaborated with a non-adaptive robot, i.e. the robot trajectory only depends on the learned skills and targets. In the second trial (EIB), the robot was equipped with the proposed ergo-interactive behavior (see Section II-D). In the third trial (EIB-C), the robot was equipped with ergo-interactive behavior, and a more complex environment was considered for the task. Obstacles 2 and 3 were included, which hinder the motion of the mobile base. The subjects were asked to monitor the environment and adjust the trajectory through human-robot physical interactions.

In all the trials, the subjects were required along their path to stand on a brick and move back behind obstacle 1 to avoid stepping on it. The purpose of this setting is to reproduce a cluttered environment, typical of real scenarios, in which the worker may adopt non-ergonomic configurations to collaborate with the robot.

C. Experimental Settings and Analysis

1) Parameters Settings: In *Skill Learning* (Section II-A), to ensure (1) and (2) achieve critical damping and the method has satisfactory learning results, the corresponding constants were set to $\alpha_c = 4\beta_c = 50$ and $\alpha_r = 4\beta_r = 50$, respectively, and 100 RBFs were selected to fit the nonlinear functions [23]. Since the frequency of the motion-capture device is 60 Hz and the mobile manipulator is 500 Hz, τ was set to 5 to fill the gap. In this way, the execution time of the task was about 22.5 s, which was considered a suitable average value for different subjects. It should be emphasized here that the execution time can be flexibly adjusted by changing τ offline or online to adapt to the task requirements and individual preferences.

In *Human Ergonomics* (Section II-B), by referring to the REBA score in [18], the joint limits q^H_{max} and the desired joints q^H_d of the back, shoulder, and elbow flexion-extension were set to $\left[q^H_{\mathrm{max},1}, q^H_{\mathrm{max},2}, q^H_{\mathrm{max},3}\right] = \left[90^\circ, 180^\circ, 180^\circ\right]$ and $\left[q^H_{d,1}, q^H_{d,2}, q^H_{d,3}\right] = \left[0^\circ, 0^\circ, 80^\circ\right]$, respectively.

In *Robot Controller* (Section II-C), to obtain a good tracking performance and avoid too high joint velocities near singularities. The parameters in (15) were set to $\boldsymbol{K} = 0.01 \cdot \mathrm{diag}(10, 10, 10, 1, 1, 1)$, $\boldsymbol{W}_1 = 500 \cdot \mathrm{diag}(2, 2, 2, 1, 1, 1)$, $\boldsymbol{W}_2 = \mathrm{diag}(10, 10, 10, 0.5, 0.5, 0.5, 0.5, 0.5, 0.5)$, and $k = 1$. $\boldsymbol{W}_3$ in (16) was set to $\boldsymbol{W}_3 = \boldsymbol{I}^9$.

In *Robot Ergo − Interactive Behaviour* (Section II-D), For task execution, the watersheds for the areas of ergonomics and supervision are empirically set to $\gamma_{\mathrm{thr}} = 0.1$ (11) and $\|\boldsymbol{e}\|_{\mathrm{thr}} = 0.4\,m$ (12), respectively. The gain for $\boldsymbol{F}_{ergo}$ is empirically set to $\boldsymbol{K}_e = 100\boldsymbol{I}^{3\times3}$ and $\boldsymbol{F}_c = 30\boldsymbol{I}^3$ (13), respectively. The parameters of the admittance controller are set to $\boldsymbol{K}_d = k_i\boldsymbol{I}^{3\times3}$, in which $k_i = 200$, and $\boldsymbol{D}_d = 2 \cdot \mathrm{diag}(\sqrt{k_i})$ (19) by referring to [24] and the requirements of real scenarios. To ensure the completion of the task and put the box in the target area, the adjustment of the trajectory is prohibited in the last 30 % of the task (16-22.5 s).

2) Skill Learning Evaluation: The learning effect of the Riemmannian DMP depends on the positive constants (α, β) and the time scale factor τ in (1) and (2), and the number N and weight distribution ω of RBFs in (3). To evaluate the skill-learning results under these parameters, this letter employs two indicators: reachability and similarity proposed in [19]. The former is used to evaluate the convergence ability of the Riemmannian DMP based on the absolute position and angle errors w.r.t. the Cartesian and Riemannian space trajectories, respectively. The latter is applied by using Pearson's correlation coefficient to assess the correlation between the generalization and the demonstration trajectories, which is related to the imitative ability of the Riemmannian DMP.

3) Human Ergonomics and Preferences: To evaluate the outcome of the multi-subject experiments, the proposed ergonomic index (see (11)) was considered and the subjects were asked to fill in the NASA-TLX [25] to assess their workload. Statistical analysis was carried out to compare all the trials based on the two-sided Wilcoxon Signed-Rank Test, with a significance level equal to 0.05.

D. Experimental Results

1) Human-Robot Task Execution Via Skill Transfer: In Fig. 7, the demonstrated, reproduced, and generalized trajectories (w.r.t. three new targets) are represented in each subplot. The position (left column) along x-, y-, and z- axes were processed in Cartesian space with the average reachability of 0.1418 mm, 0.1688 mm, and 0.5851 mm, respectively. For the quaternion-based orientation (right column), the angle-quaternion and axis-quaternion were encoded in Cartesian space and 2-D sphere manifold with the average reachability of 0.2807° and 0.8297°, respectively. The average similarity of the Cartesian and Riemannian space skills are all close to 1.

[2] A video of the experiments is available at https://youtu.be/_TRHz_TlbfQ

[3] The experimental protocol was approved by the ethics committee ASL Genovese N.3 (Protocol IIT_HRII_ERGOLEAN 156/2020). Participants signed written informed consent.

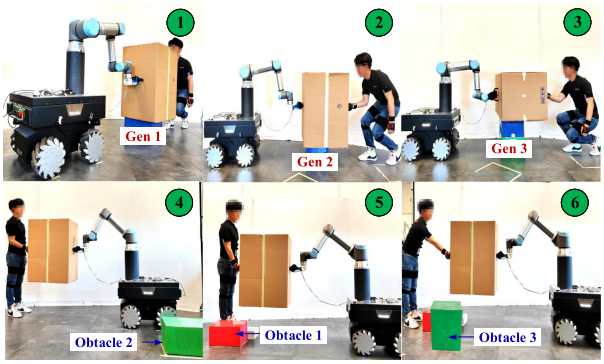

Fig. 8. Snapshoots of human-robot co-carrying (1: Final state of Gen1, 2: Final state of Gen2, 3: Final state of Gen3, 4: Initial state with obstacle 2, 5: The subject stand on the brick with obstacle 1 nearby, 6: The subject move back behind obstacle 1 with obstacle 3 nearby).

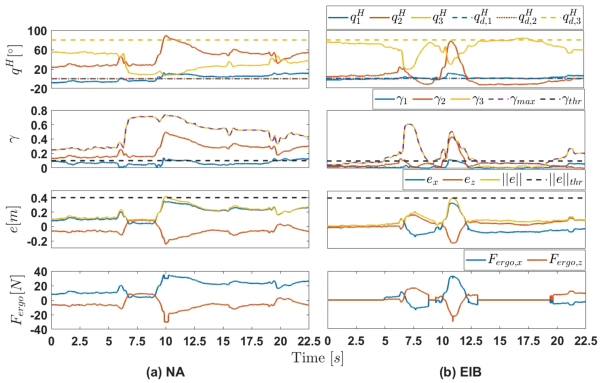

Fig. 9. Results of the co-carrying experiment without (a) and with (b) the robot ergo-interactive behaviour (Section II-D), i.e. NA and EIB trials, for one subject.

The experimental results show that the developed Riemannian-based DMP method provides a feasible way for skill learning in multi-spaces. It is worth noting that the learning module needs to be run only once, and each generalization can be realized based on the new starts, targets, and execution time, without repeated robot teaching and additional time-consuming processes. Thus, the human-robot co-carrying for different targets was conducted via LfHD (see Fig. 8, first row).

2) Robot Ergo-Interactive Behaviour: Fig. 9 depicts the results of one subject, as an example, in trials NA (left column) and EIB (right column), respectively. The rows of the plot show the current and desired angles of the human upper body (q_1^H for the back, q_2^H for the shoulder, and q_3^H for the elbow), the corresponding ergonomic indexes γ, distances $\|\boldsymbol{e}\|$, and forces $\boldsymbol{F}_{ergo}$, respectively. As shown in Fig. 9(a), the human partner followed the robot's trajectory, but its posture was not ergonomic. The related angles were far from their desired ones, especially q_3^H which leads to a high ergonomic index $\gamma_{\max}$. On the other hand, thanks to the robot ergo-interactive behavior, as shown in Fig. 9(b), the angles kept their values around the desired ones. In particular, the starting point of the learned trajectory is moved to the most ergonomic position for the human partner, ensuring a correct posture from the beginning of the task. Correspondingly, $\gamma_{\max}$ was quite low throughout the task. At 5-12.5 s, the human partner stood on the brick (see Fig. 8.5) and moved backward

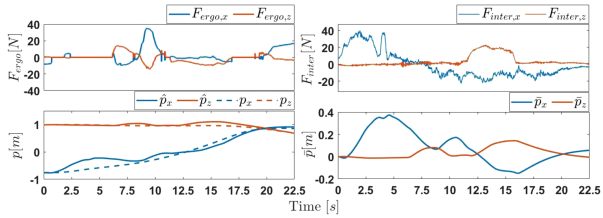

Fig. 10. Results of the co-carrying experiment with the robot ergo-interactive behaviour and cluttered environment, i.e. EIB-C trial, for one subject.

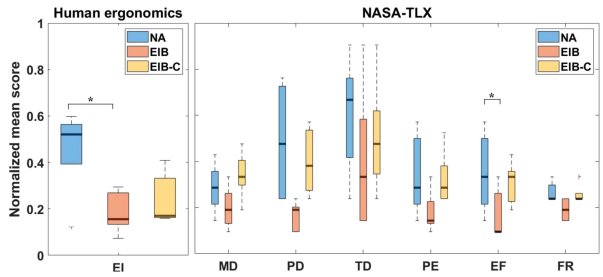

Fig. 11. Boxplots for the human upper body ergonomics and NASA-TLX results among all subjects for the experimental conditions NA, EIB, and EIB-C, respectively. Rated aspects are the ergonomic index (EI) $\gamma_{\max}$, and from NASA-TLX: Mental demand (MD), physical demand (PD), temporal demand (TD), performance (PE), effort (EF), and frustration (FR). (*: $p < 0.05$).

to avoid Obstacle 1 (see Fig. 8.6), successively. In NA, this led to an unrecoverable raise of $\gamma_{\max}$, while in EIB, the ergonomic index was first increased and then quickly decreased thanks to the robot adaptation. Accordingly, $\|\boldsymbol{e}\|$ was quite high in NA but the corresponding $\boldsymbol{F}_{ergo}$ was not applied, while it fulfilled its role in EIB, by correcting the human posture.

Fig. 10 shows, for one subject as an example, the ergonomic and interaction forces $\boldsymbol{F}_{ergo}$ and $\boldsymbol{F}_{inter}$, position of the learned and updated trajectory $\boldsymbol{p}$ and $\hat{\boldsymbol{p}}$, and corresponding displacements $\bar{\boldsymbol{p}} = \hat{\boldsymbol{p}} - \boldsymbol{p}$. At the beginning of the EIB-C trial, the robot adjusted the subject to its best ergonomic posture. Then, the subject observed the environment and pulled the robot along the $+x$- axis to avoid the obstacle while still keeping an ergonomic posture. Accordingly, $\boldsymbol{F}_{inter}$ increased while $\boldsymbol{F}_{ergo}$ remained low. At 0-7.5 s, the robot had a 0.4 m response to the maximum 40 N force. Then, a combined force of $\boldsymbol{F}_{ergo}$ and $\boldsymbol{F}_{inter}$ caused a 0.2 m offset of the robot at 7.5-12.5 s. Similarly, along the $+z$-axis, the human partner lifted up the box with a nearly 20 N force at 12-16 s, and the displacement response was nearly 0.2 m.

The experimental results validate the feasibility of the proposed ergonomic and interactive HRC framework, the robot inherits the learned collaborated skills and exhibits quick and good adaptability to human interactions and ergonomics needs. It is important to note here that the adaptability of robots depends on the parameters of the admittance-like controller, their empirical settings w.r.t. the task requirements.

3) Statistical Analysis: In Fig. 11, the results of the statistical analysis are depicted for trials NA, EIB, and EIB-C, respectively. Let us first focus on the boxplots of NA (blue) and EIB (red), with the same experimental environment. The ergonomic index shows a significant reduction between NA and EIB, i.e. 69.18% ($p = 0.0313$) proving the capability of the robot ergo-interactive behavior to enhance human physical ergonomics. The results from the NASA-TLX show statistically significant differences

in EF ($p = 0.0313$) and approaching significant differences in PD ($p = 0.0625$) and PE ($p = 0.0625$), with reductions of 58.32%, 53.36%, and 53.43%, respectively. This suggests the potential of the robot ergo-interactive behavior in reducing the subjects' perceived effort and improving performance. For the other scores, the p-values were 0.1250, 0.1250, and 0.2500 for MD, TD, and FR, respectively. It should be noted that all the tasks were executed with the same duration and the human motion was guided by the robot, hence, significant differences were not envisaged in these scores.

Furthermore, let us observe the boxplots of EIB-C (yellow), compared to NA. Although significant reductions are not shown in perceived workload (NASA-TLX) most likely due to the higher complexity of this condition, subjects still exhibit better ergonomics ($p = 0.1250$). On this basis, the experimental results further validated the effectiveness of the framework, the robot guided humans to complete the task while enhancing their ergonomics in HRC.

IV. Conclusion

In this work, we proposed an ergonomic and interactive HRC framework based on a Riemannian-based DMP, an online quantitative human ergonomics model, and a robot interaction controller. The framework blends the complementarity between humans and robots so that they can supervise each other during HRC. Humans exploit their flexibility to adjust the learned trajectory to environmental conditions while the robot, aware of human ergonomics, keeps correcting human posture through the shared task. The effectiveness of the framework was evaluated by conducting a comparative human-robot co-carrying experiment with and without the proposed ergo-interactive control. Experimental results show that the robot inherits the demonstrated skills and exhibits good adaptation in dynamic situations, ensuring a significant ergonomic enhancement for the human partner.

A limitation of the proposed framework is that ergonomics is only considered in the sagittal plane of the human upper body at the kinematic level. Future work will integrate more information including both physical (e.g., joint load, fatigue, etc.) and cognitive (e.g., attention, stress, etc.) factors into the framework to increase its generalizability and applicability to other tasks. Moreover, to enhance its customizability, the possibility of online adjusting the execution time based on human preferences will be considered.

Acknowledgment

This work was carried out at the Human-Robot Interfaces and Interaction (HRI2) Laboratory, Istituto Italiano di Tecnologia (IIT), Genoa, Italy.

References

[1] A. Ajoudani, A. M. Zanchettin, S. Ivaldi, A. Albu-Schäffer, K. Kosuge, and O. Khatib, "Progress and prospects of the human–robot collaboration," *Auton. Robots*, vol. 42, pp. 957–975, 2018.

[2] D. Mukherjee, K. Gupta, L. H. Chang, and H. Najjaran, "A survey of robot learning strategies for human-robot collaboration in industrial settings," *Robot. Comput.- Integr. Manuf.*, vol. 73, 2022, Art. no. 102231.

[3] B. Nemec, N. Likar, A. Gams, and A. Ude, "Human robot cooperation with compliance adaptation along the motion trajectory," *Auton. Robots*, vol. 42, pp. 1023–1035, 2018.

[4] A. Al-Yacoub, Y. Zhao, W. Eaton, Y. M. Goh, and N. Lohse, "Improving human robot collaboration through force/torque based learning for object manipulation," *Robot. Comput.- Integr. Manuf.*, vol. 69, 2021, Art. no. 102111.

[5] M. Khoramshahi and A. Billard, "A dynamical system approach to task-adaptation in physical human—robot interaction," *Auton. Robots*, vol. 43, pp. 927–946, 2019.

[6] P. Evrard, E. Gribovskaya, S. Calinon, A. Billard, and A. Kheddar, "Teaching physical collaborative tasks: Object-lifting case study with a humanoid," in *Proc. IEEE-RAS 9th Int. Conf. Humanoid Robots*, 2009, pp. 399–404.

[7] G. J. Maeda, G. Neumann, M. Ewerton, R. Lioutikov, O. Kroemer, and J. Peters, "Probabilistic movement primitives for coordination of multiple human–robot collaborative tasks," *Auton. Robots*, vol. 41, pp. 593–612, 2017.

[8] K. Qian, X. Xu, H. Liu, J. Bai, and S. Luo, "Environment-adaptive learning from demonstration for proactive assistance in human–robot collaborative tasks," *Robot. Auton. Syst.*, vol. 151, 2022, Art. no. 104046.

[9] D. Vogt, S. Stepputtis, S. Grehl, B. Jung, and H. B. Amor, "A system for learning continuous human-robot interactions from human-human demonstrations," in *Proc. IEEE Int. Conf. Robot. Automat.*, 2017, pp. 2882–2889.

[10] W. Wang, R. Li, Y. Chen, Z. M. Diekel, and Y. Jia, "Facilitating human–robot collaborative tasks by teaching-learning-collaboration from human demonstrations," *IEEE Trans. Automat. Sci. Eng.*, vol. 16, no. 2, pp. 640–653, Apr. 2019.

[11] L. Peternel, T. Petrič, E. Oztop, and J. Babič, "Teaching robots to cooperate with humans in dynamic manipulation tasks based on multi-modal human-in-the-loop approach," *Auton. Robots*, vol. 36, pp. 123–136, 2014.

[12] J. d. Kok et al., "Work-related musculoskeletal disorders: Prevalence, costs and demographics in the EU," *Eur. Agency Saf. Health Work*, vol. 1, 2019.

[13] M. Lorenzini, M. Lagomarsino, L. Fortini, S. Gholami, and A. Ajoudani, "Ergonomic human-robot collaboration in industry: A review," *Front. Robot. AI*, vol. 9, 2023, Art. no. 262.

[14] W. Kim et al., "Adaptable workstations for human-robot collaboration: A reconfigurable framework for improving worker ergonomics and productivity," *IEEE Robot. Automat. Mag.*, vol. 26, no. 3, pp. 14–26, Sep. 2019.

[15] I. E. Makrini, G. Mathijssen, S. Verhaegen, T. Verstraten, and B. Vanderborght, "A virtual element-based postural optimization method for improved ergonomics during human-robot collaboration," *IEEE Trans. Automat. Sci. Eng.*, vol. 19, no. 3, pp. 1772–1783, Jul. 2022.

[16] L. F. C. Figueredo, R. C. Aguiar, L. Chen, S. Chakrabarty, M. R. Dogar, and A. G. Cohn, "Human comfortability: Integrating ergonomics and muscular-informed metrics for manipulability analysis during human-robot collaboration," *IEEE Robot. Automat. Lett.*, vol. 6, no. 2, pp. 351–358, Apr. 2021.

[17] L. v. d. Spaa, M. Gienger, T. Bates, and J. Kober, "Predicting and optimizing ergonomics in physical human-robot cooperation tasks," in *Proc. IEEE Int. Conf. Robot. Automat.*, 2020, pp. 1799–1805.

[18] S. Hignett and L. McAtamney, "Rapid entire body assessment (REBA)," *Appl. Ergonom.*, vol. 31, no. 2, pp. 201–205, 2000.

[19] Z. Liao, G. Jiang, F. Zhao, Y. Wu, Y. Yue, and X. Mei, "Dynamic skill learning from human demonstration based on the human arm stiffness estimation model and Riemannian DMP," *IEEE/ASME Trans. Mechatron.*, vol. 28, no. 2, pp. 1149–1160, Apr. 2023.

[20] M. Lorenzini, W. Kim, and A. Ajoudani, "An online multi-index approach to human ergonomics assessment in the workplace," *IEEE Trans. Hum.-Mach. Syst.*, vol. 52, no. 5, pp. 812–823, Oct. 2022.

[21] F. Tassi and A. Ajoudani, "Multi-modal and adaptive control of human-robot interaction through hierarchical quadratic programming," early access, 2023, doi: 10.21203/rs.3.rs-2401107/v2.

[22] H. Seraji and R. Colbaugh, "Improved configuration control for redundant robots," *J. Robotic Syst.*, vol. 7, no. 6, pp. 897–928, 1990.

[23] A. J. Ijspeert, J. Nakanishi, H. Hoffmann, P. Pastor, and S. Schaal, "Dynamical movement primitives: Learning attractor models for motor behaviors," *Neural Computation*, vol. 25, no. 2, pp. 328–373, 2013.

[24] C. Ott, *Cartesian Impedance Control of Redundant and Flexible-Joint Robots*. Berlin, Germany: Springer, 2008.

[25] S. G. Hart and L. E. Staveland, "Development of NASA-TLX (task load index): Results of empirical and theoretical research," *Adv. Psychol.*, vol. 52, pp. 139–183, 1988.